Available online at www.sciencedirect.com

jmr&t Journal of Materials Research and Technology

www.jmrt.com.br

Original Article

Enhancing the tensile performance of ultra-high-performance concrete through novel curvilinear steel fibers

*Jae-Jin Kim, Yun Sik Jang, Doo-Yeol Yoo**

Department of Architectural Engineering, Hanyang University, 222 Wangsimni-ro, Seongdong-gu, Seoul 04763, Republic of Korea

ARTICLE INFO

Article history:
Received 9 March 2020
Accepted 18 May 2020
Available online 5 June 2020

Keywords:
Ultra-high-performance concrete
Novel reinforcement
Steel fibers
Pullout resistance
Curvature
Tensile performance

ABSTRACT

This study developed a novel curvilinear steel fiber to improve the tensile behavior of ultra-high-performance concrete (UHPC) and to mitigate the stress concentration observed in conventional deformed steel fibers. To achieve this, four curvilinear steel fibers of different curvatures (0.02–0.10 mm range) and a commercial smooth, straight steel fiber were employed. The average and equivalent bond strengths could be improved using the curvilinear steel fibers than the straight fiber from the UHPC matrix. The tensile performance of UHPC was improved by using the curvilinear fibers of curvature (κ) up to 0.04 mm. The tensile strength and energy absorption capacity were significantly increased up to 52% and 174%, respectively, by replacing the straight steel fiber to the moderately curved steel fibers with $\kappa = 0.04$ mm, which is the optimum fiber type. The highly curved steel fibers, i.e., with curvatures beyond 0.04 mm, slightly deteriorated the tensile performance because of the poorer fiber dispersibility and excessive matrix damage. A comparison of the pullout and tensile parameters showed that the equivalent bond strength of inclined steel fibers in UHPC is the most appropriate indicator for predicting the tensile performance.

1. Introduction

Richard and Cheyrezy first introduced a reactive powder concrete in the mid-1990s to improve the strength of ordinary concrete [1]. This has since been developed into ultra-high-performance fiber-reinforced concrete (UHPFRC) and has not only been extensively studied but also employed in numerous countries including the United States, Germany, Japan, and South Korea [2–5]. Since an ultra-high-performance concrete (UHPC) is fabricated by using very fine ingredients rather than coarse aggregate, a high particle packing density is achieved, leading to compacted microstructures. Hence, it has excellent mechanical properties, such as an extraordinarily high compressive strength (≥150 MPa) and durability [6,7], owing to which, it has attracted worldwide attention for building and infrastructure applications [8].

Although its tensile strength is much higher than that of ordinary concrete, the compressive strength of the UHPC remains low, which makes it extremely brittle because a large

* *Corresponding author.*
E-mail: dyyoo@hanyang.ac.kr (D. Yoo).

https://doi.org/10.1016/j.jmrt.2020.05.072

Table 1 – Mixture proportions.

W/B[b]	Unit weight (kg/m^3)					
	Water	Cement	Silica fume	Silica sand	Silica flour	SP[a]
0.2	160.3	788.5	197.1	867.4	236.6	52.6

Note: W/B, water-to-binder ratio; SP, superplasticizer.

[a] Superplasticizer includes 30% solid (= 15.8 kg/m^3) and 70% water (= 36.8 kg/m^3).

[b] W/B is calculated by dividing total water content (160.3 kg/m^3 + 36.8 kg/m^3) by total amount of binder (788.5 kg/m^3 + 197.1 kg/m^3).

amount of its energy is rapidly dissipated in the failure state [9]. To overcome these limitations and meet the design tensile strength of 8 MPa and ductility in accordance with the recommendations of the international codes [2,3], discontinuous fibers such as the micro straight steel fiber, are generally incorporated. Although the commercially available steel fibers for the UHPC have a high tensile strength of over 2000 MPa [10], the micro straight steel fiber of 0.2 mm diameter and 13 mm length, which is widely used exhibits a maximum tensile stress of only 981 MPa [11], i.e., its capacity is not fully developed. In other words, the straight fibers in the UHPC are currently being pulled out with less than half of the maximum tensile strength, and hence, a new type of steel fiber is required to maximize the reinforcing effect. Accordingly, numerous studies [12–21] have been conducted for enhancing the reinforcing efficiency of the steel fibers in the UHPC.

Wille and Naaman [12] reported that the highest equivalent bond strength of up to 47 MPa, which is 4–5 times greater than that of the straight steel fiber, can be obtained by embedding high-strength deformed steel fibers, i.e., hooked and twisted fibers, in the UHPC. Tai et al. [13,14] conducted fiber pullout tests using straight, hooked, and twisted steel fibers in the UHPC under static and impact loading conditions, ranging from 0.018 to 1800 mm/s, at various inclination angles between 0° and 60°. They reported that the deformed steel fibers exhibited enhanced pullout resistance in comparison with the straight steel fiber. Similarly, Wille et al. [15] reported that the hooked and twisted steel fibers could also effectively enhance the tensile and flexural performance of UHPC. However, recent studies by Yoo et al. [16] showed that, although the hooked fibers in UHPC clearly exhibited higher pullout resistance than the straight fiber, it exhibited a relatively poorer flexural performance owing to premature matrix cracking that occurs near the end hooks of the inclined fibers. Similarly, Kim and Yoo [17,18] observed a stress concentration at the end hook of the hooked fiber in the UHPC during the pullout process using the digital image correlation method. Xu et al. [19] and Yoo and Kim [20] attempted to mitigate the stress concentration by developing half-hooked steel fibers, which they achieved by cutting one end hook of the hooked fiber. However, although the UHPC samples with the half-hooked fibers exhibited better tensile performance than that with hooked fibers, its performance was still poorer than those reinforced using the straight and twisted fibers. Therefore, Kim et al. [21] developed a new type of curvilinear fiber by bending the commercially available straight fiber and reported several useful findings based on the single fiber pullout tests: (1) the pullout resistance of the curvilinear steel fiber is higher than that of the straight fiber; (2) the effectiveness increases with the curvature, regardless of the inclination angles and loading rates; and (3) the matrix spalling area in the developed curvilinear fibers is relatively smaller than that in the other conventional deformed, i.e., hooked and twisted, fibers. These observations imply that the curvilinear steel fiber is a highly potential and novel alternative to the conventional UHPC reinforcement using the straight and deformed steel fibers. However, its impact on the tensile performance of the composites must be examined prior to the practical use of such a novel type of reinforcing fiber, as it is influenced by various factors including fiber dispersibility, random orientation, and effective matrix volume covering the fibers.

Table 2 – Chemical compositions and physical properties of cement and silica fume.

Composition [%] (mass)	Type I Portland cement	Silica fume
CaO	61.33	0.38
Al_2O_3	6.40	0.25
SiO_2	21.01	96.00
Fe_2O_3	3.12	0.12
MgO	3.02	0.10
SO_3	2.30	–
Specific surface area [cm^2/g]	3413	200,000
Density [g/cm^3]	3.15	2.10

Accordingly, this study evaluated the tensile performance of the UHPC samples with the newly developed curvilinear steel fibers to verify their feasibility and effectiveness. Four types of steel fibers of different curvatures, ranging from 0.02 to 0.10 mm, were adopted along with a commercial straight steel fiber for comparison, and the same fiber volume fraction of 1.5% was applied to all the tested samples. The tensile test results of UHPFRC were verified through an examination of the number of fibers located at the localized crack planes. The correlation between the fiber pullout and tensile parameters was analyzed and compared to determine the most proper indicator for predicting the tensile performance of UHPC reinforced with the straight and curvilinear steel fibers.

2. Materials and methods

2.1. *Raw materials and mixture proportions*

An identical UHPC mixture proportion was applied for all the specimens in both pullout and direct tensile tests. The details of the used materials and mixture proportion are provided in Table 1. Type I Portland cement and silica fume were adopted as the cementitious materials, and their chemical compositions and physical properties are provided in

Table 3 – Geometrical and physical properties of steel fibers.

	d_f (mm)	l_f (mm)	Aspect ratio (l_f /d_f)	Density (g/cm^3)	f_{ft} (MPa)	E_f (GPa)
S-fiber	0.300	30.0	100.0	7.9	2580	200

Note: S, straight steel fiber; d_f, fiber diameter; l_f, fiber length; f_{ft}, tensile strength of fiber; E_f, elastic modulus of fiber.

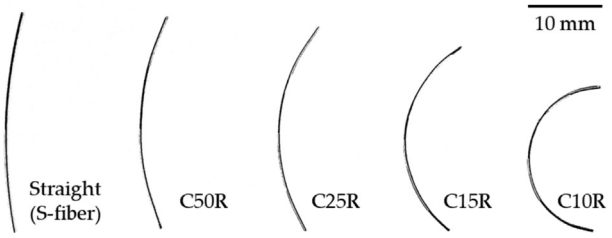

Fig. 1 – The detailed geometric of the used steel fibers.

Table 2. As suggested in previous studies [22,23], the coarse aggregate, which causes deterioration of fiber pullout resistance and post-cracking tensile performance, was excluded in the UHPC mixture. Silica sand with a grain size in the range of 0.2–0.3 mm and silica flour with an average diameter of approximately 4.2 μm were adopted as the filler. A UHPC mixture proportion optimized with high-strength steel fibers based on the study by Park [24], and a low water–binder (W/B) ratio of 0.2 was adopted. Furthermore, polycarboxylate superplasticizer (SP) with density of 1.01 g/cm^3 was used as a water-reducing admixture to ensure the proper flowability of the fresh UHPC, as it exhibits insufficient flowability due to the low W/B ratio and high amounts of fine ingredients [25]. All used steel fibers were fabricated from the commercially available straight steel fiber of 0.3 mm diameter and 30 mm length. Its detailed physical properties, such as density, tensile strength (f_{ft}), and elastic modulus (E_f), are summarized in Table 3.

To improve the bridging capability of the fiber, various types of curvilinear steel fibers were used. The detailed geometrical properties of the used steel fibers are described in Fig. 1. The labels used for the curvilinear steel fibers include information regarding the fiber type, radius of curvature, and fiber orientation. The straight and curvilinear fibers are denoted by the capital letters, S and C, respectively. The subsequent numeral in company with the capital letter R indicates the radius of curvature. The aligned and inclined conditions denote the capital letters A and I, respectively. For example, the C50R-A indicates the aligned curvilinear steel fiber with a radius of curvature of 50 mm.

2.2. *Mixing sequence and specimen fabrication*

To fabricate fresh UHPC, we first mixed the dry ingredients (namely cement, silica fume, silica sand, and silica flour) for 10 min using a Hobart-type mixer to obtain a well-dispersed mixture. Next, water that was premixed with SP added dry ingredients was added and mixed for 10 min, to make a flowable mixture. For pullout test specimens, fresh UHPC was poured into the mold to which the steel fiber fixed, and for direct tensile test specimens, the steel fibers were incorporated into the fresh UHPC mortar. The fabricated UHPC mortar was poured into the pullout and tensile specimen molds and cured for 48 h at room temperature, after which, the hardened specimens were demolded. Subsequently, the specimens were steam-cured in a water tank at a high temperature of 90 ± 2 °C for 48 h according to the FHWA recommendations [26].

Pullout test specimen whose height, width, and cross-sectional area were 75 mm, 40 mm, and 25 mm × 25 mm, respectively, was used, as shown in Fig. 2a. A polyethylene (PE) film was set at the middle cross-section of the pullout test specimen to precisely investigate the pullout behavior of the steel fiber, excluding the matrix contribution. A single steel fiber was placed in the middle of the cross-section of the specimens. To arrange the fibers to be pulled out from the same side in all specimens, the shorter embedment length was set to 10 mm on one side, while the other side had a longer embedment length of 20 mm. To investigate the effect of the fiber inclination, considering the random fiber orientation in the composites, both aligned and inclined fiber samples were prepared: thus, the capital letters A and I indicate the two inclination angles, namely aligned (0°) and inclined (45°), respectively. The notations of the fiber pullout specimens are summarized in Table 4.

The direct tensile test was conducted using specimens, whose the cross-sectional area of each tensile specimen was 30 mm × 13 mm and the gauge length was 80 mm, based on the recommendations of the Japan Society of Civil Engineers (JSCE), as illustrated in Fig. 2b [27]. Although steel fibers with 2% volume fraction were normally used for the commercial products and direct tensile specimens in a previous study [28], in this study, steel fibers with 1.5% volume fraction were used not only for fabricating the UHPFRC composites but also to verify if the 0.5% steel fibers could be reduced by replacing with the curvilinear steel fibers and to minimize the fiber ball effect due to the fiber deformation (curvature). Before the test, the surfaces of the tensile specimens were coated with polyurethane after the heat curing process to effectively detect the microcracks. Five specimens were fabricated for each variable in both fiber pullout and direct tensile tests to obtain more accurate test results.

2.3. *Setup for the fiber pullout and direct tensile tests*

Two types of servo controlled universal testing machines (UTMs) were utilized for the fiber pullout and direct tensile test. The experimental setups for fiber pullout and direct tensile test are shown in Fig. 3a and b. The pullout specimens were inserted into the steel grip jig and pulled vertically with

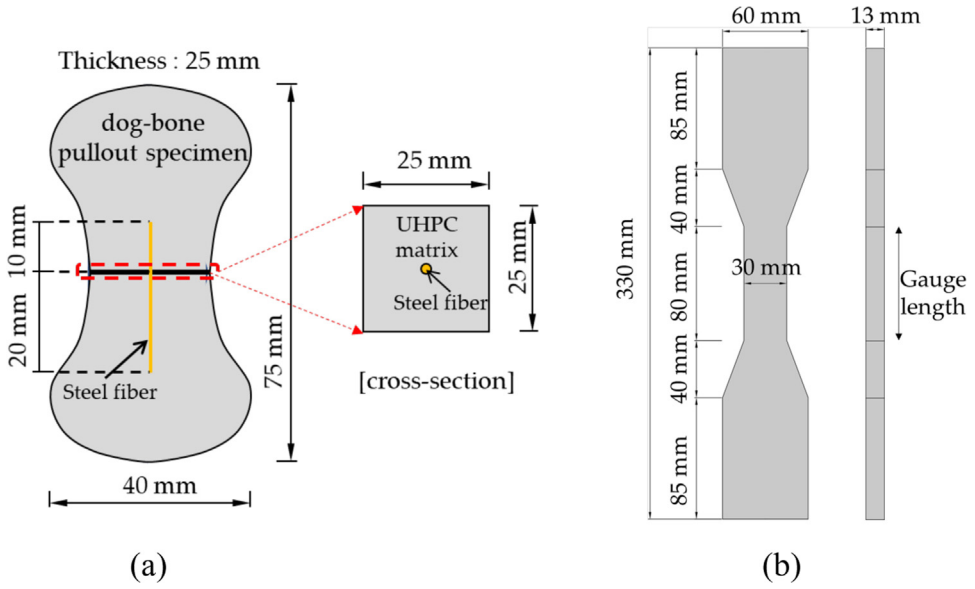

Fig. 2 – Schematic description of specimens for (a) fiber pullout test and (b) direct tensile test.

Table 4 – Test variables.

Specimens	Radius of curvature (mm)	Curvature (κ) (mm^{-1})	Fiber orientation
S-A	–	–	Aligned (0°)
C50R-A	50	0.020	
C25R-A	25	0.040	
C15R-A	15	0.067	
C10R-A	10	0.100	
S-I	–	–	Inclined (45°)
C50R-I	50	0.020	
C25R-I	25	0.040	
C15R-I	15	0.067	
C10R-I	10	0.100	

Note: S, straight steel fiber; C, curvilinear fiber; R, radius of curvature; A, aligned; I, inclined.

loading rate of 0.018 mm/s, and the fiber pullout load was measured using a load cell with a maximum capacity of 3 kN. A fixed-fixed boundary condition was applied for the fiber pullout test. In addition, since the elastic deformations of the specimens and grips were negligibly small, the displacement of the crosshead was measured and utilized as the fiber slip. A fixed-fixed boundary condition was applied for the fiber pullout test.

Likewise, a tensile specimen was inserted into the steel grip, and a uniaxial tensile load was applied with loading rates of 0.4 mm/min, and the tensile load was measured using a load cell with a maximum load capacity of 250 kN. As suggested in a previous study by Kanakubo [29], a pin-fixed boundary condition was adopted to minimize the secondary flexural stress and to ensure a centric loading condition. To measure pure elongation, an aluminum frame with two linear variable differential transformers (LVDTs) was affixed to the specimen, and the tensile strain was calculated by dividing the measured elongation with the gauge length of 80 mm.

3. Results and discussion

3.1. *Fiber pullout behaviors*

3.1.1. *Average pullout load versus slip response*

Fig. 4 shows the average pullout load and slip curves of the straight and curvilinear steel fibers in the UHPC at two different inclination angles, namely 0° and 45°. The results were similar to those previously reported by Lee et al. [30] and Tai and El-Tawil [14]: clearly, it is differed for the pullout load and slip curves according to the fiber shapes (curvatures) and inclination angles. A steeply increasing pullout load was observed in the initial debonding zone for the aligned fibers. Although the steel fibers are chemically bonded to the surrounding UHPC matrix, these bonds are relatively weak and not slip-induced [31]; therefore, the measured slip is almost zero during pullout test. In the subsequent partial debonding stage, it is observed that the steel fibers are debonded with the surrounding UHPC matrix as frictional bond stresses

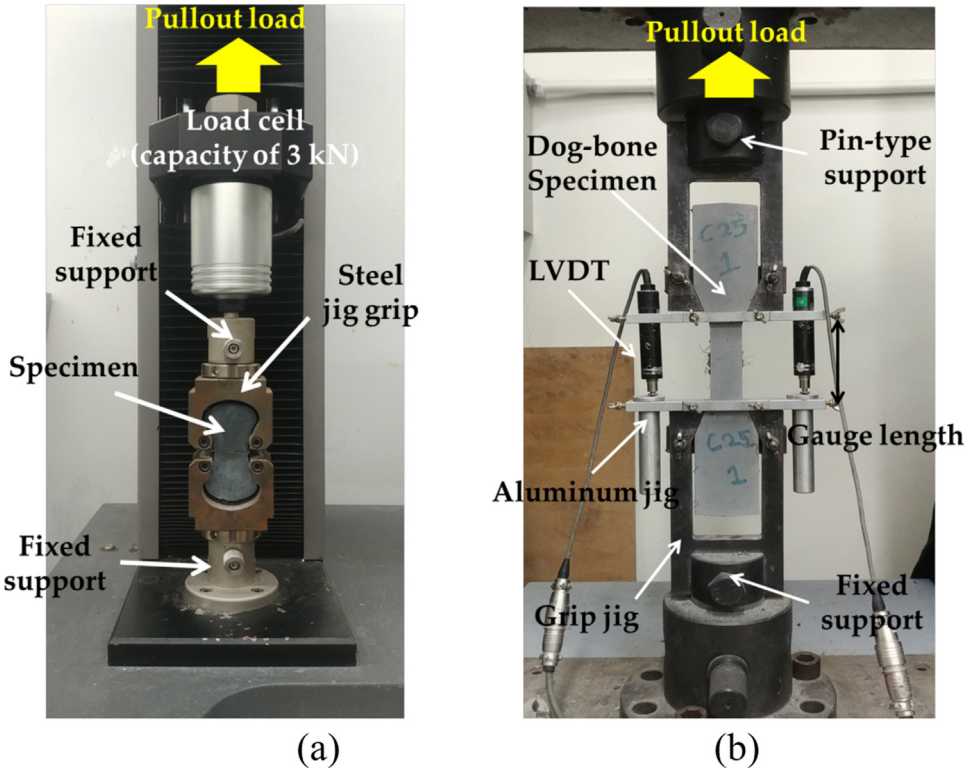

Fig. 3 – Experimental test setups: (a) pullout test machine and (b) tensile test machine.

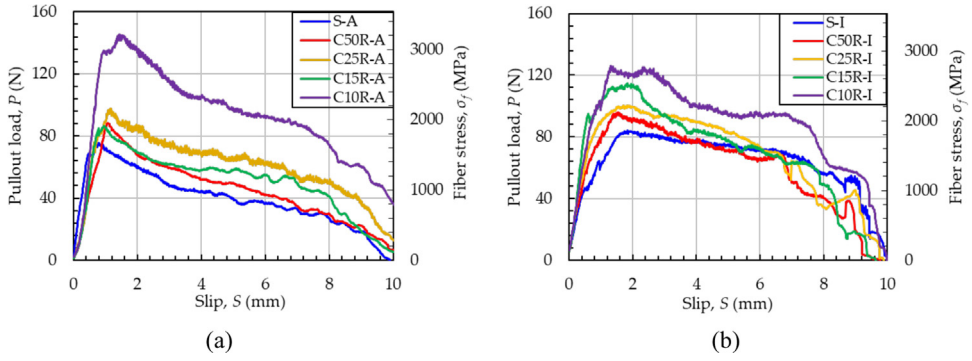

Fig. 4 – Pullout load versus slip responses curves: (a) aligned and (b) inclined steel fibers.

activate and increase. After the fiber is completely debonded, it begins to be pulled out from the matrix, leading to a gradual decrease in the pullout load due to the decrease in the embedment length until the end of slip.

Fig. 4b clearly shows the different shapes of the pullout load-slip curves for the inclined samples: it is observed that these samples generally provide a higher maximum pullout load and slip capacity than the aligned fiber specimens, except for C10R; this is consistent with the findings of the previous studies [30,32]. In general, when a conventional cement mortar is used as a matrix, a sudden decrease in pullout load is observed due to a Poisson's ratio effect [31]; however, such effect was not observed for the UHPC matrix due to the characteristics of UHPC which has very few pores and compact structure [33]. Furthermore, although the pullout parameters such as the bond strength and energy absorption capacity were affected by the curvatures of the fibers, the shapes of the load-slip curves of the straight and curvilinear steel fibers were reasonably similar, regardless of their degrees of curvature and inclination angles. Generally, the curvilinear fibers exhibited better pullout resistance than the straight ones under both aligned and inclined conditions, which was observed to increase with their curvature.

3.1.2. *Effects of fiber curvature and inclination angle on the pullout parameters*

The results of the single fiber pullout tests are highly sensitive to the manufacturing process of specimens and testing conditions. For instance, although fibers should be embedded in the UHPC matrix the same length of 10 mm for all pullout

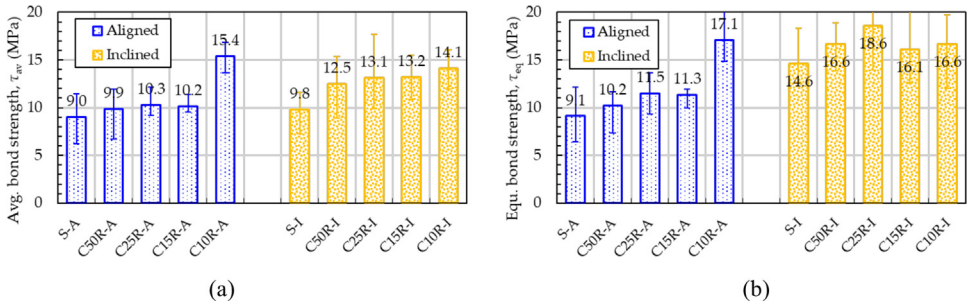

Fig. 5 – The results of bond strength: (a) average bond strength and (b) equivalent bond strength.

Table 5 – Summary of pullout parameters of fibers depending on fiber types, fiber orientations.

Fiber type	Parameters	Fiber orientation	
		Aligned	Inclined
S-fiber	P_{max} (N)	81.45 (19.65)	88.40 (14.08)
	W_p ($\times 10^{-3}$ J)	395.75 (111.32)	632.09 (100.83)
	$\sigma_{f,max}$ (MPa)	1152.34 (278.03)	1250.56 (199.12)
	τ_{av} (MPa)	9.01 (2.21)	9.79 (1.70)
	τ_{eq} (MPa)	9.13 (2.61)	14.58 (2.49)
C50R	P_{max} (N)	89.93 (33.15)	101.50 (19.62)
	W_p ($\times 10^{-3}$ J)	450.75 (191.64)	592.44 (137.46)
	$\sigma_{f,max}$ (MPa)	1272.21 (771.72)	1435.91 (685.67)
	τ_{av} (MPa)	9.88 (5.76)	12.51 (6.05)
	τ_{eq} (MPa)	10.20 (5.86)	16.63 (7.65)
C25R	P_{max} (N)	103.10 (11.10)	106.34 (20.71)
	W_p ($\times 10^{-3}$ J)	611.74 (315.92)	654.74 (178.77)
	$\sigma_{f,max}$ (MPa)	1458.57 (806.57)	1504.45 (292.98)
	τ_{av} (MPa)	10.31 (5.76)	13.15 (3.21)
	τ_{eq} (MPa)	11.48 (6.47)	18.58 (4.84)
C15R	P_{max} (N)	93.11 (8.70)	120.16 (7.99)
	W_p ($\times 10^{-3}$ J)	504.53 (41.62)	710.59 (98.81)
	$\sigma_{f,max}$ (MPa)	1317.30 (598.68)	1699.86 (766.49)
	τ_{av} (MPa)	10.17 (4.61)	13.19 (6.16)
	τ_{eq} (MPa)	11.35 (5.14)	16.09 (7.85)
C10R	P_{max} (N)	156.86 (20.86)	145.46 (12.81)
	W_p ($\times 10^{-3}$ J)	945.57 (222.55)	933.99 (150.61)
	$\sigma_{f,max}$ (MPa)	2219.08 (1024.77)	2057.80 (933.56)
	τ_{av} (MPa)	15.41 (7.01)	14.13 (6.49)
	τ_{eq} (MPa)	17.11 (7.96)	16.64 (7.98)

Note: P_{max}, maximum pullout load; W_p, pullout work; $\sigma_{f,max}$, maximum fiber tensile stress; τ_{av}, average bond strength; τ_{eq}, equivalent bond strength; (), standard deviation.

specimens, as the fiber pullout resistance is directly related to the embedment length, even a small error of less than 1 mm in the fiber embedment length could cause large deviations. Therefore, for a more reliable data analysis, the pullout performance was compared in terms of the average and equivalent bond strengths – which can reflect the actual embedded length, rather than the maximum pullout load and pullout energy. The results of the fiber pullout test are summarized in Table 5 and Fig. 5. Among the various pullout parameters, the average and equivalent bond strengths, which are related to the peak point and energy absorption capacity, respectively, are shown in Fig. 5.

The average bond strength was calculated using the following formula, which is based on the maximum pullout load: assuming that the frictional bond stress is uniformly distributed throughout the embedment length of a fiber, the average bond strength can be calculated by dividing the maximum pullout load with the bonding area between the fiber and matrix, which is given in Eq. (1).

$$\tau_{av} = \frac{P_{max}}{\pi d_f L_E} \quad (1)$$

where τ_{av} is the average bond strength in MPa, P_{max} is the maximum pullout load in N, d_f is the fiber diameter in mm, and L_E is the initial embedded length of the fiber in mm.

The equivalent bond strength is based on the pullout energy and calculated by assuming that the interfacial shear stress is distributed equally along the entire embedment length of the fiber. The equivalent bond strength is calculated by the following Eq. (2).

$$\tau_{eq} = \frac{2W_p}{\pi d_f L_E^2} \quad (2)$$

where W_p is the fiber pullout energy in Nm, where τ_{eq} is the equivalent bond strength in MPa.

The straight steel fiber in the UHPC exhibited an average bond strength of 9.01 MPa. The aligned curvilinear fibers clearly exhibited higher average bond strengths than the straight fiber, and these values were observed to increase as the curvature increased from 9.88 MPa for C50R to 15.41 MPa for C10R. Similarly, the average bond strengths of the aligned fibers tended to increase by a maximum of 71% for the C10R fibers as compared with the straight fiber; the inclined straight fiber exhibited an average bond strength of 9.79 MPa, which slightly increased as the curvature was increased, i.e., from 12.51 MPa for C50R to 14.13 MPa for C10R. Except for the C10R sample, the inclined fibers exhibited higher average bond strengths than the aligned fibers because of the snubbing effect, which was more dominant than the matrix spalling effect at the 45° angle [30]. Furthermore, the inclined straight fiber exhibited an increase of 8.5%, while the C50R, C25R, and C15R samples exhibited an increase in the average bond strengths in the range of 3.1–29.7%, compared with the aligned fibers. Synthetically, the bond strengths exhibited an increasing tendency with the increase in the curvature for both the aligned and inclined states.

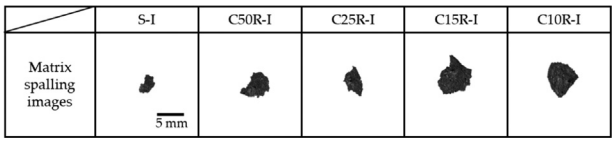

Fig. 6 – Typical matrix spalling images of the cross-sectional surface after completion of pullout test.

The equivalent bond strengths of the curvilinear fibers were larger than those of the straight fibers: the aligned fibers exhibited a general increasing tendency with increasing curvature, i.e., from 10.20 MPa for C50R to 17.11 MPa for C10R. The equivalent bond strength of the inclined straight fiber was 14.58 MPa, while that of the inclined C25R sample was highest at 18.58 MPa, which is 27% higher than the former. On the other hand, there was no consistent increase in the equivalent bond strengths of the inclined fibers with curvature increase: for example, the inclined C15R and C10R fibers exhibited smaller equivalent bond strengths than the inclined C25R fiber, which could be due to the increased matrix spalling effect.

If the maximum fiber stress exceeds the fiber tensile strength during the pullout test, the fiber will be fractured before it is completely pulled out. Therefore, the maximum fiber stress, which is calculated by Eq. (3), can be used to determine the suitability of the fibers in concrete, and is based on the maximum pullout load and the cross-sectional area of the fiber.

$$\sigma_{f,\max} = \frac{P_{\max}}{A_f} \tag{3}$$

where $\sigma_{f,\max}$ is the maximum tensile stress of the fiber, $P_{\max}$ is the maximum pullout load, A_f is the fiber cross-sectional area ($= \pi d_f^2/4$), and d_f is the fiber diameter.

The maximum fiber stress was observed to increase with increasing curvature due to the increase in the pullout resistance. The maximum stress for the aligned fibers varied from 1152.3 MPa for the straight fiber to 2219.1 MPa for the C10R; similarly, under the 45° inclined condition, it gradually increased from 1250.6 MPa for the straight fiber to 2057.8 MPa for the C10R. As these values are lower than the tensile strength of the fiber (2580 MPa) provided by the manufacturer (Table 3), the straight and curvilinear steel fibers could be completely pulled out from the UHPC matrix without any breakage.

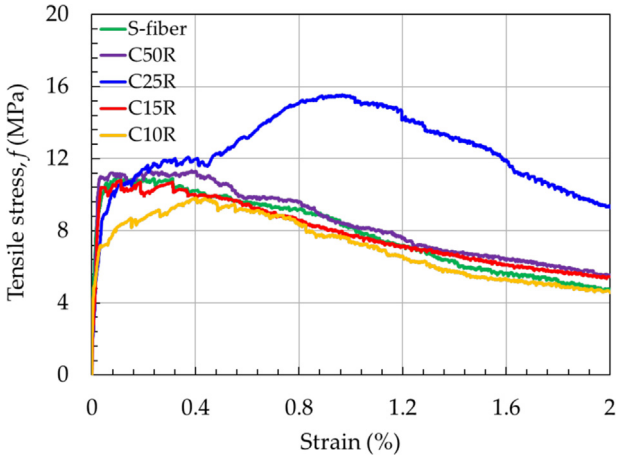

Fig. 8 – Average tensile stress versus strain curves.

3.1.3. *Analysis on the matrix spalling property*

The generation of matrix spalling reduces the pullout resistance during fiber pullout reducing the interfacial bonding area between the fiber and surrounding matrix. Thus, underestimated average and equivalent bond strengths were measured because these parameters are calculated based on the initial embedment length, L_E. For the aligned fiber specimens, matrix spalling was not clearly observed regardless of fiber shape (curvature); therefore, it was concluded that there has almost been no spalling. However, the inclined fibers exhibited some matrix spalling during the pullout process from the UHPC matrix. Therefore, the degree of matrix spalling was analyzed only for the inclined fiber samples. Typical matrix spalling images of the cross-sectional surface after completion of pullout test are shown in Fig. 6, and the measured average matrix spalling areas of the inclined fibers in the UHPC are summarized in Fig. 7. As the curvilinear fibers were bent over its entire length, the stress concentration was reduced, which in turn mitigated the matrix damage and

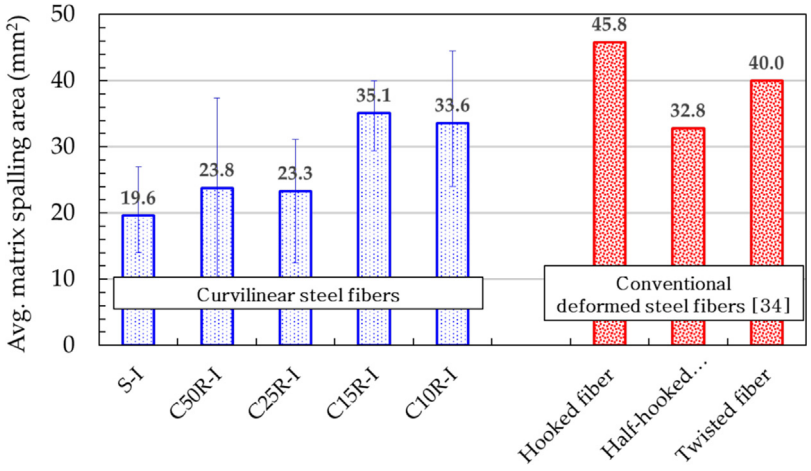

Fig. 7 – Comparative matrix spalling areas of inclined fibers in UHPC [34].

Table 6 – Summary of tensile results.

Fiber type	Tensile strength, σ_{pc} (MPa)	Strain capacity, ε_{pc} (%)	g-value (kJ/m^3)
S-fiber	10.85 (0.98)	0.386 (0.16)	39.80 (13.70)
C50R	12.16 (1.32)	0.503 (0.35)	55.29 (35.50)
C25R	16.50 (2.66)	0.978 (0.30)	109.27 (26.49)
C15R	11.33 (1.25)	0.310 (0.05)	31.59 (6.49)
C10R	9.96 (1.23)	0.448 (0.12)	38.48 (13.51)

(), standard deviation.

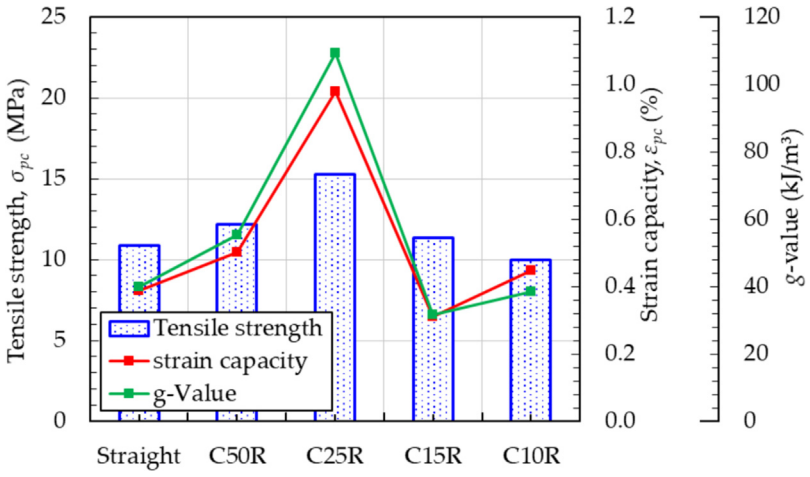

Fig. 9 – Summary of tensile strength, strain capacity, and g-value of UHPFRCs.

spalling as compared with the conventional deformed, i.e., twisted, hooked, and half-hooked, steel fibers. However, the spalling area in the highly curved fiber samples, such as the C15R and C10R, was greater than in the others (namely the straight and moderately curved fibers), and their spalling areas were smaller than those of the hooked and twisted steel fibers but similar to the that of the half-hooked fiber (Fig. 7).

3.2. *Direct tensile behaviors of UHPFRC*

3.2.1. *Average tensile stress versus strain response*

Fig. 8 shows the average tensile stress and strain curves of all the tested samples. According to the curvature of the steel fibers, the evidently different tensile stress–strain curves were obtained. The UHPC samples with C25R fibers noticeably exhibited the best tensile performance, followed by the C50R fiber. In contrast, the C10R fibers, which has highest curvature, exhibited poorer tensile performance than even the straight fibers. The result is inconsistent with the results of the single fiber pullout tests, wherein better fiber pullout resistance was observed in steel fibers with a higher degree of curvature. The strain-hardening, a phenomenon in which tensile stress increases after initial matrix crack, were observed in most of the UHPC samples such as the C50R, C25R, and C10R fibers. Although there is no obvious increase in the tensile stress for the UHPC samples with the straight and C15R fibers after matrix cracking, the tensile stress was maintained close to the peak value during some strain section and then gradually decreased.

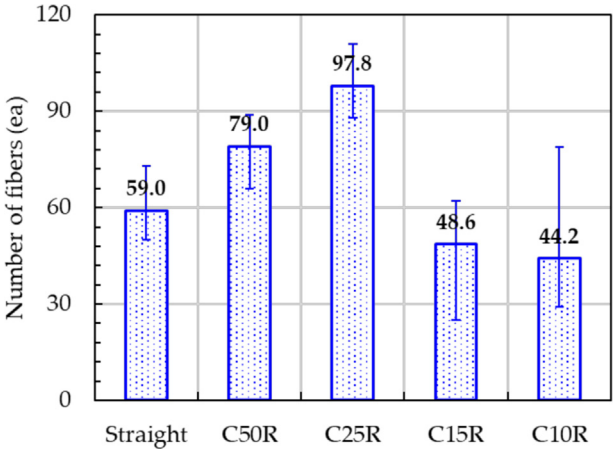

Fig. 10 – Number of fibers at cross-sectional area near localized crack.

Although the curvature of the fibers had little effect on the tensile stiffness of the test samples before the first crack, the post-cracking tensile stiffness was different: the C25R fiber specimens clearly exhibited the highest post-cracking stiffness, whereas the C10R fiber specimens exhibited the lowest. Meanwhile, the other test specimens, such as the straight, C50R, and C15R fibers, exhibited similar post-cracking tensile stiffness, which was between that of the C25R and C10R fiber samples. The poor dispersibility of the highly curved steel fibers could be the main reason for this lower post-cracking stiffness. Furthermore, during the mixing process,

the fire ball phenomenon becomes more prominent as the curvature of the increases. As the number of fibers reinforcing the UHPC matrix is closely related to the post-cracking tensile performance in terms of the strength and stiffness, the tensile cracks can locally occur in sections where the fiber reinforcement is weak when the fibers are not evenly dispersed. In addition, severe damage to the matrix during the pullout process of the fibers could be another reason for the poorer tensile performance. Similarly, poorer tensile performance of UHPC reinforced with the conventional deformed steel fibers was due to the high mechanical anchorage effect owing to their premature pullout from the matrix [34]. For instance, matrix splitting cracks are typically formed at the crack surface toward the end of the fiber because of the extremely high mechanical anchorage of the twisted steel fiber in the UHPC matrix [14]. The hooked steel fibers were also not fully straightened in the composites because premature matrix cracking occurs due to a stress concentration close to the end hook of the fibers [32]. In the case of C15R and C10R fibers, the non-straightened fibers were easily found in the localized crack planes, especially when they were severely inclined, mainly due to the increased mechanical anchorage effect from the higher curvature. The abovementioned investigation shows that the matrix spalling area of the inclined C15R and C10R fibers is similar to that of the deformed steel fibers (Fig. 7) and greater than the straight and moderately curved ones. Thus, the tensile performance of the UHPC samples with highly curved steel fibers was deteriorated.

3.2.2. *Effect of fiber curvature on the tensile parameters*

In order to investigate the effects of fiber curvature on the tensile behavior of the UHPC, several important tensile parameters such as post-cracking tensile strength (σ_{pc}), strain capacity (ε_{pc}), and energy absorption capacity up to the peak load (g-value) were examined, and they are summarized in Table 6 and Fig. 9. The UHPC samples with the C25R fibers clearly exhibited the best tensile performances in terms of all tensile parameters, followed by those with the C50R fibers. This indicates that the tensile performance of UHPFRC could be improved by using the curvilinear steel fibers up to a curvature of 0.04 mm. For the UHPC samples with straight fibers exhibited tensile strength of 10.85 MPa, strain capacity of 0.39%, and g-value of 39.80 kJ/m^3. The highest tensile strength, strain capacity, and g-value were observed to be 16.5 MPa, 0.98%, and 109.3 kJ/m^3 in the C25R fiber samples, respectively. These tensile parameters were higher by 52%, 153%, and 174%, respectively, than those of the straight fiber samples.

However, no significant benefits of increasing the fiber curvature on the tensile parameters were observed beyond these values (C25R). A slightly poorer tensile performance was observed in the curvilinear fiber samples, i.e., C15R and C10R. This result, i.e., the highest tensile strength in the C25R fiber specimen, is inconsistent with those of the single fiber pullout tests. The highest average bond strength, which is directly related to the post-cracking tensile strength, was found in the specimens of the C10R fibers. As mentioned earlier, this is because of the matrix damage caused by the deformation of fibers, random orientation, and ununiformed dispersion. The inclined fibers generally led to damages in the matrix during the pullout process and the matrix spalling area in the

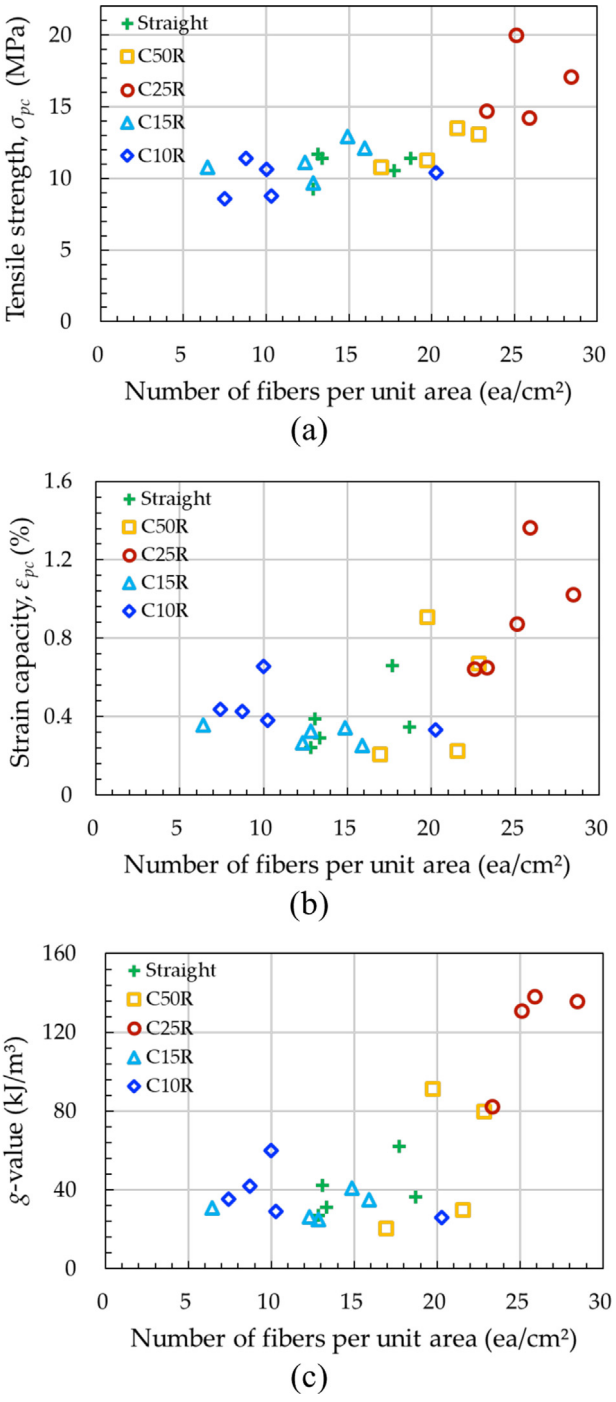

Fig. 11 – Relationships between tensile parameters and number of fibers per unit area: (a) tensile strength, (b) strain capacity, and (c) g-value.

C10R and C15R fibers is as large as that in the conventional deformed fibers (Fig. 7). Moreover, owing to the fiber ball effect, the localized cracks were more easily generated through the weakest section of the specimen (with less fibers). This implies that the highly curved steel fibers (C15R and C10R) are inappropriate for improving the tensile performance of UHPC.

According to a previous study, fiber-reinforced concrete (FRC) is considered to be at the highest tensile performance

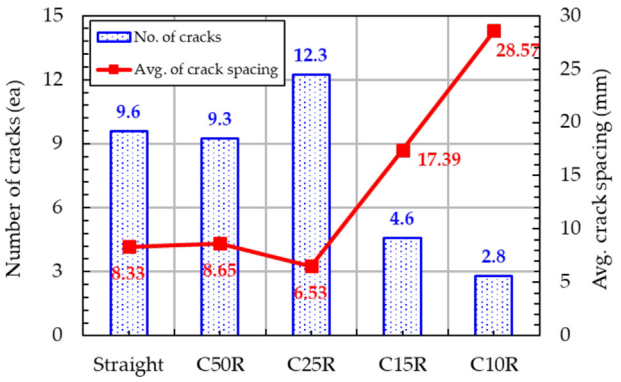

Fig. 12 – Summary of number of cracks and average crack spacing.

level if its g-value is higher than 50 kJ/m^3 [35]. The UHPC samples with the C50R and C25R fiber used in this study exhibited a g-value greater than 50 kJ/m^3. In particular, the highest g-value of 109.3 kJ/m^3 for the C25R fiber samples was two times higher than the required value of 50 kJ/m^3 [35]. Moreover, although the UHPC samples with conventional steel fibers, i.e., straight, twisted, and hooked fibers, which exhibited a g-value of approximately 55–94 kJ/m^3 with a volume fraction of 2–3% [35], the UHPC samples in this study contained only steel fibers with a volume fraction of 1.5%. Therefore, synthetically, the C25R fiber is an adequate alternative to the existing reinforcing fiber type for enhancing the tensile performance of UHPC.

3.2.3. *Correlations among the tensile parameters and the number of fibers at the localized crack of samples*

Increasing the fiber curvature was observed to efficiently improve the tensile performance of the UHPC only up to 0.04 mm. The post-cracking tensile behaviors of tested samples were directly affected by the number of fibers at the localized crack planes of them; therefore, the number of fibers at the localized crack planes was examined and summarized in Fig. 10. The actual average number of fibers per unit area (ea/cm^2) was found to be 15.1, 20.3, 25.7, 12.5, and 11.3 ea/cm^2 for the UHPC samples with straight, C50R, C25R, C15R, and C10R fiber, respectively. For the UHPC samples with the C15R and C10R fibers, the number of fibers on the localized cracks was clearly smaller than those with the other types of fibers, mainly due to the fiber ball phenomenon, leading to poorer dispersibility and random orientation of the fibers. The more inclined fibers damaged the surrounding matrix more severely, thereby causing the degradation of the reinforcing effect. However, the moderately curved fibers such as the C50R and C25R increased the number of detected fibers at the localized cracks because both ends of the fiber, positioned perpendicularly to the cracks, can be detected owing to the curvature.

The correlations among the tensile parameters, (i.e., the tensile strength, strain capacity, and g-value), and the number of fibers per unit area for all the tested samples are illustrated in Fig. 11. The tensile strength of UHPFRC is observed to increase with the increase in the number of fibers in general, although the tendency was not linear (Fig. 11a). The C50R and C25R fiber samples exhibited a relatively linear increase with increasing number of fibers at the localized cracks, whereas the C15R and C10R fiber samples showed no significant increase or decrease in the tensile strength with the number of fibers. Similarly, the strain capacity and g-value of only the moderately curved, i.e., C50R and C25R, fiber samples exhibited an increasing tendency with the number of fibers detected at the localized cracks (Fig. 11b and c). On the contrary, for the highly curved C15R and C10R fiber samples, the parameters were quite consistent regardless of the number of fibers per unit area owing to the more severe matrix damage, caused by a premature pullout failure before reaching their ultimate capacity. Thus, the tensile parameters were not influenced by the number of highly curved fibers located at the localized crack planes.

3.2.4. *Analysis of cracks and failure modes*

The average number of cracks and crack spacings are summarized in Fig. 12, and the typical failure cracking patterns and failure modes are shown in Fig. 13. The number of cracks

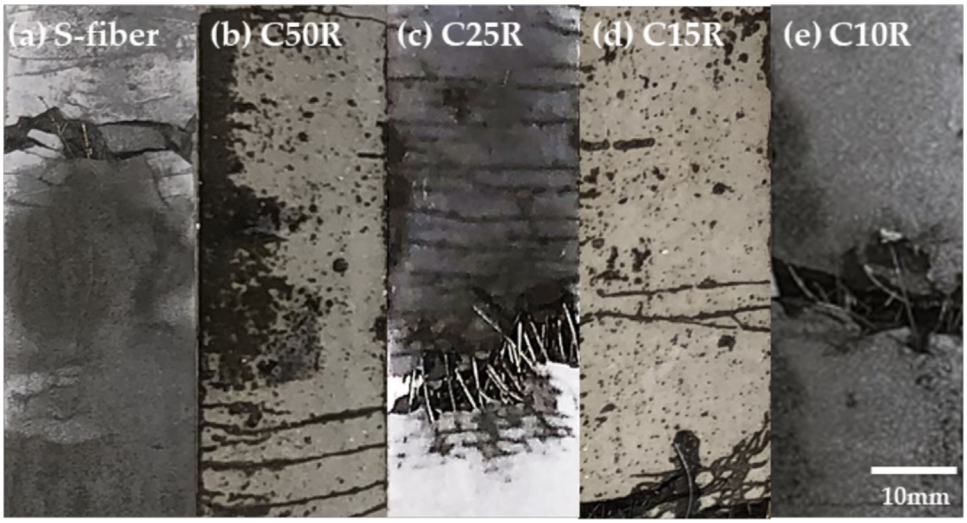

Fig. 13 – Cracking pattern and failure mode of UHPFRC: (a) S-fiber, (b) C50R, (c) C25R, (d) C15R, and (e) C10R.

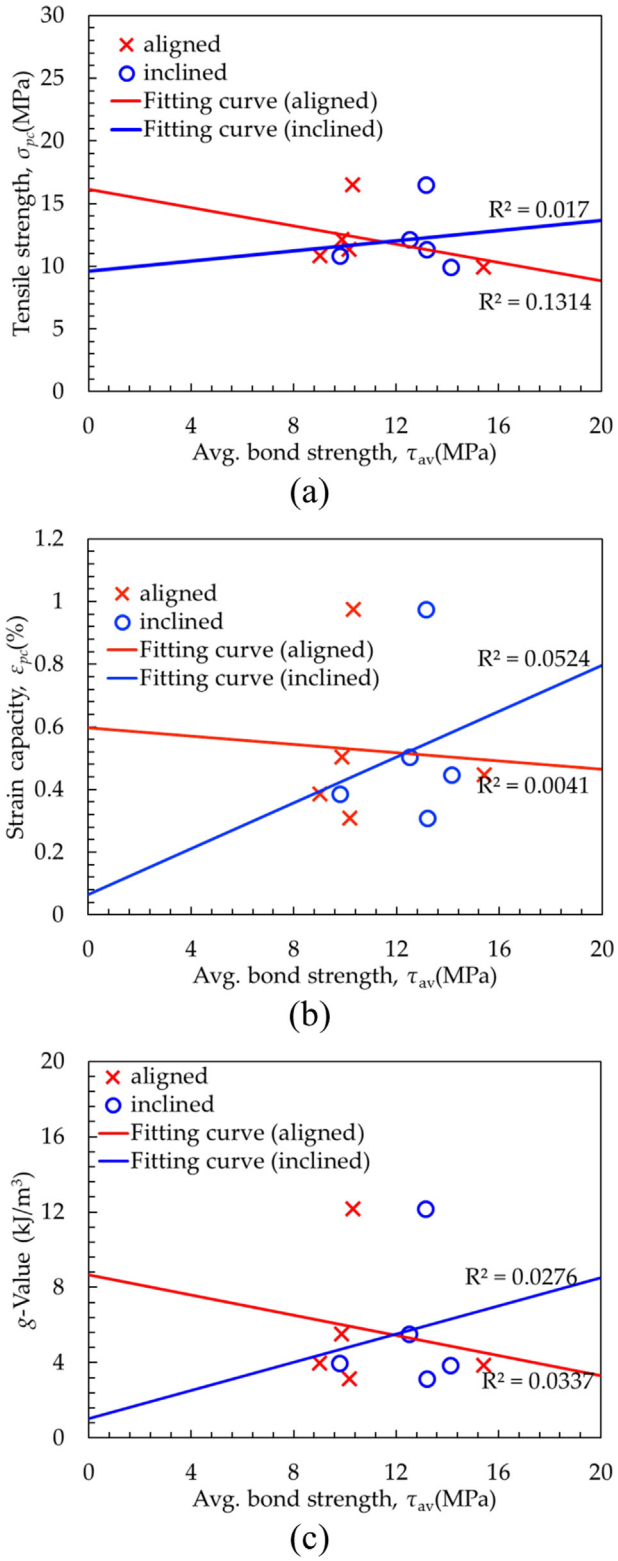

Fig. 14 – Correlation between average bond strength and the tensile parameters: (a) tensile strength, (b) strain capacity, and (c) *g*-value.

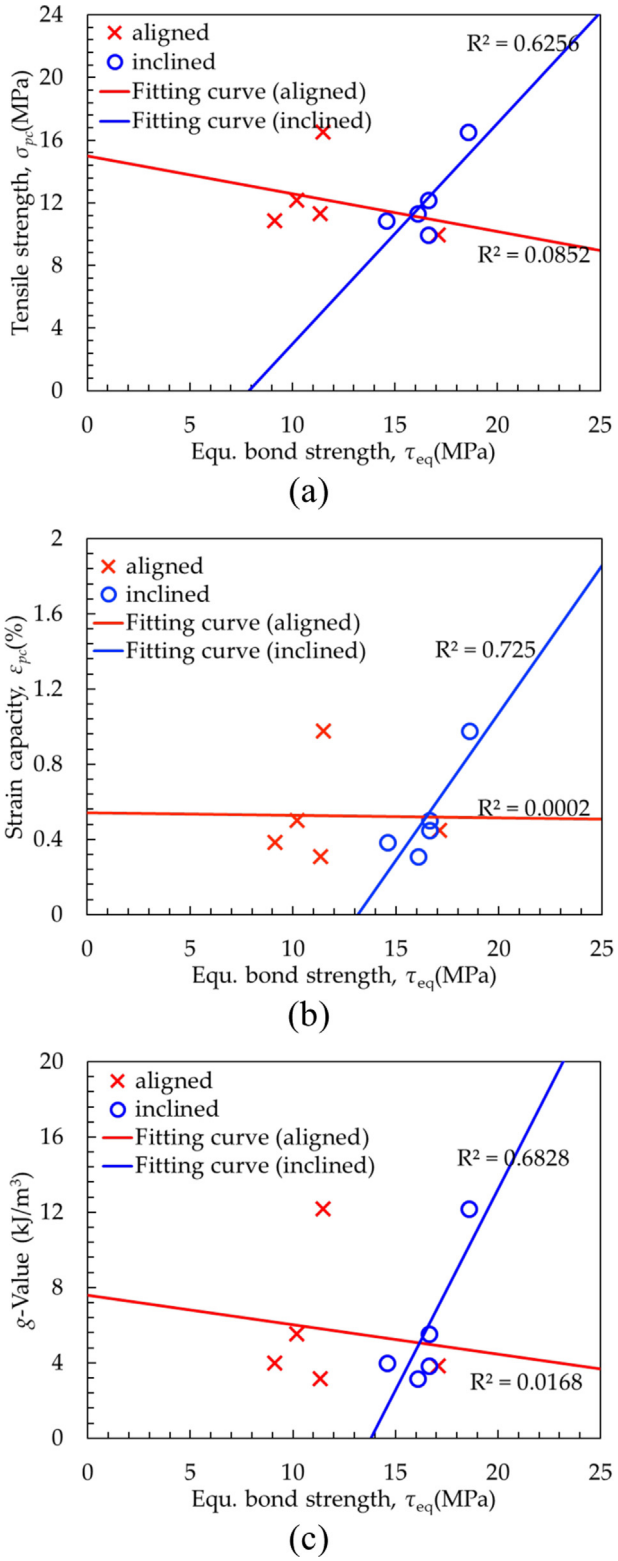

Fig. 15 – Correlation between equivalent bond strength and the tensile parameters: (a) tensile strength, (b) strain capacity, and (c) *g*-value.

is inversely proportional to the spacing between the cracks in the tested samples; in other words, a generation of larger number of cracks caused a smaller average crack spacing. The highest number of cracks and smallest average crack spacing were found in the UHPC samples with the C25R fibers, and they were 12.3 ea and 6.53 mm, respectively. Thus, the C25R fiber samples exhibited the best tensile performance with effective stress transmission to the composites. As the number of microcracks is related to deformability, a better cracking behavior of the C25R fiber samples led to a higher strain capacity. Although the straight fiber samples exhibited the second-best crack performance with the number of cracks and an average crack spacing of 9.6 ea and 8.33 mm, respectively, these values were similar to those with the C50R fibers. However, the UHPC samples with the highly curved fibers, i.e., the C15R and C10R fibers, exhibited lower number of cracks, which became more significant with the increase in curvature; this is consistent with the results of the tensile parameters. Thus, the moderately curved fibers are also effective in terms of the cracking performance.

3.2.5. *Correlation between single fiber pullout and tensile behaviors*

To investigate the correlation between the single fiber pullout and tensile behaviors, the pullout parameters, i.e., the average and equivalent bond strengths, and the tensile parameters, i.e., the tensile strength, strain capacity, and *g*-value, were compared as shown in Figs. 14 and 15. While the tensile parameters of the aligned fibers tended to decrease with increasing average bond strength, those of the inclined fibers exhibited a tendency to increase (Fig. 14). Similarly, although the tensile parameters of the aligned fibers tended to decrease with increasing equivalent bond strength, those of the inclined fibers exhibited a tendency to increase (Fig. 15). This is because, while fabricating the UHPFRC, the steel fibers are randomly oriented in the matrix and the steel fibers inclined by approximately 30°–45° form the largest distribution of fiber orientations [36]. Moreover, the most fitting curves for the average bond strength exhibited very low coefficient of determination (R^2) values of less than 0.1 (Fig. 14), whereas those for the equivalent bond strength of the inclined fibers exhibited relatively higher R^2 values in the range 0.63–0.73. Therefore, the equivalent bond strength of the inclined straight or curvilinear steel fibers in UHPC is considered to be the most appropriate indicator for predicting the tensile performance of UHPFRC, rather than the average bond strength and aligned fiber cases.

4. Conclusion

In this study, a novel curvilinear steel fiber was developed to improve the tensile performance of the UHPC. For determining the optimum fiber curvature, both single fiber pullout and tensile tests were conducted for fibers with various curvatures, ranging from 0.02 to 0.1 mm. The commercially available smooth, straight steel fiber was also included for comparison. By comparing the pullout and tensile parameters, the most proper indicator among the pullout parameters to predict the tensile performance of UHPFRC was suggested. Based on the test results and discussion, the following conclusions can be drawn:

1) The curvilinear fibers exhibited higher average and equivalent bond strengths than the straight fiber, regardless of the inclination angle. The bond strengths of the aligned fibers generally increased with increasing fiber curvature, whereas the moderately curved (C25R) fiber exhibited the highest equivalent bond strength at 45° inclination.
2) The tensile performance of the UHPC can be improved by replacing the straight steel fiber reinforcements with the curvilinear steel fibers of curvature up to 0.04 mm. The C25R fiber with a curvature of 0.04 mm exhibited the best tensile performance, and its tensile strength and *g*-value were increased by 52% and 174%, respectively, compared with those of the straight fiber. At the fiber volume fraction of 1.5%, the UHPC samples with C25R fibers achieved a *g*-value of 109.3 kJ/m^3, which is two times greater than the required value (50 kJ/m^3) for the highest FRC level.
3) In contrast to the fiber pullout test result, the tensile performance of UHPC reinforced with the highly curved, i.e., C15R and C10R, fibers was slightly deteriorated, mainly due to their poorer dispersibility and excessive matrix damage. Moreover, a lower number of fibers at the localized crack planes was detected for the highly curved fiber samples as compared to the straight or moderately curved fiber samples.
4) The tensile parameters of the UHPC samples with straight or moderately curved, i.e., C50R and C25R, fibers increased with an increasing number of fibers at the localized cracks, whereas the highly curved fiber samples exhibited quite consistent tensile parameters, regardless of the number of fibers.
5) The equivalent bond strength of the inclined straight or curvilinear steel fibers in UHPC was the most proper indicator for predicting the tensile performance of UHPFRC rather than the average bond strength or aligned fiber cases.

Conflict of interest

None declared.

Acknowledgements

This research was supported by a Grant (19CTAP-C152069-01) from Technology Advancement Research Program funded by Ministry of Land, Infrastructure and Transport of Korean government.

REFERENCES

[1] Richard P, Cheyrezy M. Composition of reactive powder concretes. Cement Concr Res 1995;25(7):1501–11.
[2] AFGC. Ultra high performance fibre-reinforced concretes, Interim Recommendations. Bagneux, France: AFGC Publication; 2013.
[3] ACI Committee 239. Ultra-high performance concrete. Toronto, Ontario, Canada: ACI Fall Convention; 2012.

[4] JSCE. Recommendations for design and construction of ultra-high strength fiber reinforced concrete structures (draft). Tokyo, Japan: Japan Society of Civil Engineers; 2004.
[5] KCI-M-12-003. Design recommendations for ultra-high performance concrete K-UHPC. Seoul: Korea Concrete Institute (KCI); 2012.
[6] Spasojevic A. Structural implications of ultra-high performance fiber reinforced concrete in bridge design. EPFL; 2008 [Ph.D. thesis].
[7] Habel K, Gauvreau P. Response of ultra-high performance fiber reinforced concrete (UHPFRC) to impact and static loading. Cement Concr Res 2008;30(10):938–46.
[8] Yoo DY, Yoon YS. A review on structural behavior, design, and application of ultra-high-performance fiber-reinforced concrete slabs at early age. Constr Build Mater 2014;73:357–65.
[9] Shin HO, Yoon YS, Cook WD, Mitchell D. Effect of confinement on the axial load response of ultrahigh strength concrete columns. J Struct Eng 2015;141(6), 04014151.
[10] Graybeal BA. Flexural behavior of an ultrahigh-performance concrete I-girder. J Bridge Eng 2008;13(6):602–10.
[11] Yoo DY, Kim J, Zi G, Yoon YS. Effect of shrinkage-reducing admixture on biaxial flexural behavior of ultra-high-performance fiber-reinforced concrete. Constr Build Mater 2015;89:67–75.
[12] Wille K, Naaman AE. Pullout behavior of high-strength steel fibers embedded in ultra-high-performance concrete. ACI Mater J 2012;109(4):479–87.
[13] Tai YS, El-Tawil S, Chung TH. Performance of deformed steel fibers embedded in ultra-high performance concrete subjected to various pullout rates. Cement Concr Res 2016;89:1–13.
[14] Tai YS, El-Tawil S. High loading-rate pullout behavior of inclined deformed steel fibers embedded in ultra-high performance concrete. Constr Build Mater 2017;148:204–18.
[15] Wille K, Naaman AE, El-Tawil S, Parra-Montesinos GJ. Ultra-high performance concrete and fiber reinforced concrete: achieving strength and ductility without heat curing. Mater Struct 2012;45(3):309–24.
[16] Yoo DY, Park JJ, Kim SW. Fiber pullout behavior of HPFRCC: effects of matrix strength and fiber type. Compos Struct 2017;174:263–376.
[17] Kim JJ, Yoo DY. Effects of fiber shape and distance on the pullout behavior of steel fibers embedded in ultra-high-performance concrete. Cement Concr Compos 2019;103:213–23.
[18] Kim JJ, Yoo DY. Spacing and bundling effects on rate dependent pullout behavior of various steel fibers embedded in UHPC. Arch Civ Mech Eng 2020 [in press].
[19] Xu M, Hallinan B, Wille K. Effect of loading rates on pullout behavior of high strength steel fibers embedded in ultra-high performance concrete. Cement Concr Compos 2016;70:98–109.
[20] Yoo DY, Kim S. Comparative pullout behaviors of half-hooked and commercial steel fibers embedded in UHPC under static and impact loads. Cement Concr Compos 2019;97:89–106.
[21] Kim JJ, Yoo DY, Banthia N. Benefits of curvilinear straight steel fibers on the rate-dependent pullout resistance of ultra-high-performance concrete. Cem Concr Compos 2020 [in press].
[22] Collepardi S, Coppola L, Troli R, Collepardi M. Mechanical properties of modified reactive powder concrete. ACI Spec Publ 1997;173:1–22.
[23] Ma J, Orgass M, Dehn F, Schmidt D, Tue NV. Comparative investigations on ultra-high performance concrete with and without coarse aggregates. In: Proceedings of the international symposium on ultra high performance concrete. 2004. p. 205–12.
[24] Park JJ, Kang ST, Koh KT, Kim SW. Influence of the ingredients on the compressive strength of UHPC as a fundamental study to optimize the mixing proportion. In: Proceeding of second international symposium on ultra high performance concrete. 2008. p. 105–12.
[25] Cho CG, Kim YY, Feo L, Hui D. Cyclic responses of reinforced concrete composite columns strengthened in the plastic hinge region by HPFRC mortar. Compos Struct 2012;94(7):2246–53.
[26] Graybeal BA. Material property characterization of ultra-high performance concrete (No. FHWA-HRT-06-103); 2006.
[27] JSCE. Recommendations, for design and construction of high performance fiber reinforced cement composites with multiple fine cracks (HPFRCC). Japan: Japan Society of Civil Engineers; 2008.
[28] Chun B, Yoo DY. Hybrid effect of macro and micro steel fibers on the pullout and tensile behaviors of ultra-high-performance concrete. Composites B Eng 2019;162:344–60.
[29] Kanakubo T. Tensile characteristics evaluation method for ductile fiber-reinforced cementitious composites. J Adv Concr Techonol 2006;4(1):3–17.
[30] Lee Y, Kang ST, Kim JK. Pullout behavior of inclined steel fiber in an ultra-high strength cementitious matrix. Constr Build Mater 2010;24(10):2030–41.
[31] Namman AE, Namur GG, Alwan JM, Najm HS. Fiber pullout and bond slip: I. Analytical study. J Struct Eng 1991;117(9):2769–90.
[32] Yoo DY, Chun B, Kim JJ. Effect of calcium sulfoaluminate-based expansive agent on rate dependent pullout behavior of straight steel fiber embedded in UHPC. Cement Concr Res 2019;122:196–211.
[33] Yoo DY, Banthia N, Kang ST, Yoon YS. Size effect in ultra-high-performance concrete beams. Eng Fract Mech 2016;157:86–106.
[34] Yoo DY, Kim S, Kim JJ, Chun B. An experimental study on pullout and tensile behavior of ultra-high-performance concrete reinforced with various steel fibers. Constr Build Mater 2019;206:46–61.
[35] Wille K, El-Tawil S, Naaman AE. Properties of strain hardening ultra high performance fiber reinforced concrete (UHP-FRC) under direct tensile loading. Cement Concr Compos 2014;48:53–66.
[36] Yoo DY, Kang ST, Yoon YS. Effect of fiber length and placement method on flexural behavior, tension-softening curve, and fiber distribution characteristics of UHPFRC. Constr Build Mater 2014;64:67–81.